Acta Crystallographica Section D
Biological Crystallography
ISSN 0907-4449

Structure of human semicarbazide-sensitive amine oxidase/vascular adhesion protein-1

Emma Jakobsson,[a] Joakim Nilsson,[b] Derek Ogg[b]‡ and Gerard J. Kleywegt[a]*

[a]Department of Cell and Molecular Biology, Uppsala University, Biomedical Centre, Box 596, SE-751 24 Uppsala, Sweden, and [b]Biovitrum AB, Lead Discovery, Retziusväg 2, SE-112 76 Stockholm, Sweden

‡ Present address: Karolinska Institutet, Structural Genomics Consortium, Scheeles väg 2, SE-171 77 Stockholm, Sweden.

Correspondence e-mail: gerard@xray.bmc.uu.se

Received 16 August 2005
Accepted 12 September 2005

PDB References: human SSAO, 2c10, r2c10sf; 2HP adduct, 2c11, r2c11sf.

Semicarbazide-sensitive amine oxidase (SSAO) belongs to a ubiquitous family of copper-containing amine oxidases (CuAOs). SSAO is also known as vascular adhesion protein-1 (VAP-1) and has been identified as one of the adhesion molecules involved in the leukocyte-extravasation process. The structure of a truncated soluble form of human SSAO has been solved and refined to 2.5 Å. As expected, SSAO is a homodimer with a fold typical of the CuAO family. The topaquinone (TPQ) cofactor and a copper ion characteristic of CuAOs are present in the active site, with the TPQ in the active 'off-copper' conformation. The structure reveals that a leucine residue (Leu469) located adjacent to the active site could function as a gate controlling its accessibility. An RGD motif is displayed on the surface, where it could be involved in integrin binding and possibly play a role in the shedding of SSAO from the membrane. Carbohydrate moieties are observed at five of six potential N-glycosylation sites. Carbohydrates attached to Asn232 flank the active-site entrance and might influence substrate specificity. The structure of an adduct of SSAO and the irreversible inhibitor 2-hydrazinopyridine has been solved and refined to 2.9 Å resolution. Together, these structures will aid efforts to identify natural substrates, provide valuable information for the design of specific inhibitors and direct further studies.

1. Introduction

Semicarbazide-sensitive amine oxidase (SSAO), also known as vascular adhesion protein-1 (VAP-1), is a protein with at least two functions. It acts as a monoamine oxidase catalyzing the oxidative deamination of primary amines to aldehydes, hydrogen peroxide and ammonia (Lyles, 1996; Jalkanen & Salmi, 2001; O'Sullivan *et al.*, 2004). In addition, SSAO has been shown to be identical to VAP-1, one of the adhesive molecules participating in the leukocyte-extravasation process (Smith *et al.*, 1998; Salmi & Jalkanen, 2001). Recently, it has been shown that the enzymatic activity of SSAO is essential for the transmigration step in the extravasation process (Koskinen *et al.*, 2004). SSAO activity has also been implicated in the regulation of adipocyte differentiation and glucose transport (Zorzano *et al.*, 2003), regulation of blood pressure (Göktürk, Nilsson *et al.*, 2003; Vidrio *et al.*, 2003) and elastic fibre organization (Langford *et al.*, 1999; Göktürk, Nilsson *et al.*, 2003; Sibon *et al.*, 2004). Further, elevated levels of soluble SSAO have been detected under several pathophysiological conditions, particularly in diabetes mellitus, congestive heart failure and cirrhotic liver inflammation (Boomsma *et al.*, 2003). It has been suggested that some of the complications associated with diabetes, such as retinopathy, nephropathy,

neuropathy, atherosclerosis and cardiovascular complications, may be caused by toxic products of SSAO-catalysed reactions (Ekblom, 1998; Karádi *et al.*, 2002; Salmi *et al.*, 2002; Göktürk, Garpenstrand *et al.*, 2003). However, the full picture of the physiological roles of SSAO is still unclear and it may have a number of distinct roles.

SSAO belongs to the family of copper-containing amine oxidases [CuAO; EC 1.4.3.6; amine:oxygen oxidoreductase (deaminating) (copper-containing)] and contains a copper ion and a topaquinone (TPQ) cofactor in the active site. The TPQ cofactor derives from a tyrosine that is post-translationally modified to a quinone in an autocatalytic reaction (Janes *et al.*, 1990; Klinman, 2003). SSAO is a homodimeric sialoglycoprotein of 170–180 kDa depending on the degree of glycosylation (Salmi & Jalkanen, 1996; Smith *et al.*, 1998). The enzyme exists both as a soluble protein and as a type II transmembrane protein attached to the cell surface by an N-terminal helix. Anchored SSAO molecules are released into the bloodstream by shedding from the membrane (Göktürk, Nilsson *et al.*, 2003; Abella *et al.*, 2004; Stolen *et al.*, 2004).

Tyr471 is spontaneously modified to the TPQ cofactor in the presence of dioxygen and Cu^{II} in the active site (DuBois & Klinman, 2005). The same active site catalyses the deamination reaction, which follows a ping-pong mechanism (Mure *et al.*, 2002). In the first (reductive) half-reaction the primary amine is oxidized to the corresponding aldehyde. Subsequently, molecular oxygen is reduced to hydrogen peroxide followed by release of ammonia in the second (oxidative) half-reaction (Mure *et al.*, 2002).

The physiological substrates of SSAO are not known, but methylamine and aminoacetone are believed to be among them (Lyles, 1996; Yu *et al.*, 2003; O'Sullivan *et al.*, 2004). In addition, free amino groups on certain proteins and amino sugars have been suggested as possible physiological substrates (Salmi *et al.*, 2001; Göktürk, Nilsson *et al.*, 2003; Koskinen *et al.*, 2004; Sibon *et al.*, 2004). The formation of a transient Schiff base between membrane-bound SSAO and free amino groups on the leukocyte surface has been proposed as a part of the initial tethering step of the extravasation process (Salmi *et al.*, 2001).

The three-dimensional structure of CuAOs from *Escherichia coli* (ECAO; PDB code 1oac; Parsons *et al.*, 1995), *Pisum sativum* (PSAO; PDB code 1ksi; Kumar *et al.*, 1996), *Arthobacter globiformis* (AGAO; PDB code 1av4; Wilce *et al.*, 1997), *Hanensula polymorpha* (HPAO; PDB code 1a2v; Li *et al.*, 1998), *Pichia pastoris* (PPLO; PDB code 1n9e; Duff *et al.*, 2003) and *Bos taurus* (BSAO; PDB code 1tu5; Lunelli *et al.*, 2005) have been reported. BSAO was the first mammalian CuAO structure to be reported and its sequence is 83% identical to that of human SSAO. The level of sequence identity between human SSAO and the other five CuAOs is 20–27%. A hexagonal crystal form of full-length human SSAO/VAP-1 diffracting to 3.2 Å resolution has been reported (Nymalm *et al.*, 2003) and the coordinates have recently been released (PDB codes 1pu4 and 1us1).

The availability of the three-dimensional structure of human SSAO might aid in the identification of possible physiological substrates and would increase our understanding of this multifunctional protein. Furthermore, the structure of SSAO would facilitate the design and optimization of selective inhibitors. This is relevant, since SSAO has shown potential as an anti-inflammatory drug target (Merinen *et al.*, 2005; Stolen *et al.*, 2005; Vainio *et al.*, 2005) and inhibitors of SSAO might be used to alleviate some of the complications associated with diabetes.

Here, we report the crystal structure of an N-terminally truncated soluble form of human SSAO and that of its adduct with the irreversible inhibitor 2-hydrazinopyridine (2HP). The protein was truncated to exclude the putative transmembrane region and comprises residues 29–763 of the wild-type sequence.

Table 1
Data-collection, processing, scaling and merging statistics.

Values in parentheses are for the highest resolution shell.

	SSAO holoenzyme	SSAO–2HP adduct
Space group	$P4_3$	$P4_3$
Unit-cell parameters (Å)	$a = b = 130.2$, $c = 221.5$	$a = b = 127.4$, $c = 219.4$
Resolution range (Å)	51.6–2.5 (2.64–2.5)	83.3– 2.9 (3.1–2.9)
No. of observations	656305 (70936)	339315 (30956)
No. of unique reflections	126698 (18482)	72802 (10126)
Completeness (%)	99.8 (100.0)	94.6 (90.6)
$R_{\rm merge}$†	0.10 (0.44)	0.16 (0.46)
$\langle I/\sigma(I)\rangle$	13.8 (3.2)	12.4 (2.0)
Average redundancy	5.2 (3.8)	4.7 (3.1)
NCS	2 dimers per AU	2 dimers per AU
$V_{\rm M}$‡ (Å^3 Da^{-1})	2.8	2.8
Estimated twinning fraction	0.30	0.28

† $R_{\rm merge} = \sum_h \sum_i |I_{h,i} - \langle I_h\rangle| / \sum_h \sum_i |I_{h,i}|$. ‡ Matthews (1968).

2. Materials and methods

2.1. Expression and purification

SSAO was expressed and purified as described by Jakobsson *et al.* (2005). Briefly, the protein was expressed in HEK293 and purified by GST-affinity chromatography in the first step. The GST-fusion tag was removed by GST-tagged PreScission protease (Amersham Biosciences). Subsequently, SSAO could be collected in the flowthrough in a second GST-affinity chromatography step. Finally, a gel-filtration step was performed on a column equilibrated with 150 m*M* NaCl and 50 m*M* Tris–HCl pH 7.5. The protein was concentrated to 4 mg ml^{-1} and stored in aliquots at 193 K.

2.2. Crystallization, data collection and data processing

The crystallization of the holoenzyme and subsequent data collection and data processing were carried out as reported by Jakobsson *et al.* (2005). In short, initial crystallization conditions for the holoenzyme were obtained from the high-throughput crystallization facility at the Hauptman–Woodward Institute in Buffalo (Luft *et al.*, 2003). Crystals of the holoenzyme were obtained by the hanging-drop vapour-diffusion method with 5 µl 4 mg ml^{-1} SSAO and 5 µl 0.1 *M*

Table 2
Model and refinement statistics.

	SSAO holoenzyme	SSAO 2HP adduct
Resolution range (Å)	20.0–2.5	20.0–2.9
No. of reflections	124418	69804
R value	0.204	0.215
Last recorded free *R* value	0.252	0.276
Number of atoms ($Z > 1$)	23470	21918
Protein	22300	21360
Carbohydrate	587	315
Ions ($Ca^{2+}/Cl^{-}/Cu^{2+}$)	8/8/4	8/4/30
Solvent	563	60
Average *B* factor (Å^2)	40	60
Protein	37	62
Carbohydrate	65	85
Ions (Ca^{2+}, Cl^{-}, Cu^{2+})	28	56
Solvent	29	35
From Wilson plot	48	70
R.m.s. deviations from ideal geometry†		
Bond lengths (Å)	0.010	0.009
Bond angles (°)	1.3	1.6
Protein residues	2826	2684
Ramachandran outliers‡ (%)	2.6	8.6
Packing-quality *Z* score§	−0.8	−1.0
PDB code	2c10	2c11

† Engh & Huber (1991). ‡ Kleywegt & Jones (1996*b*). § Vriend & Sander (1993).

KBr, 0.1 *M* acetate buffer pH 5.0, 38% PEG 1000 at 288 K. Crystals appeared after two to three weeks and grew to approximately 0.3 × 0.15 × 0.1 mm. Data to 3 Å, and later 2.5 Å, were collected at 100 K after flash-cooling the crystals in liquid nitrogen. To obtain the adduct with 2HP, crystals of the holoenzyme were soaked for 5 d in 40% PEG 1000, 0.1 *M* acetate pH 5.0, 80 m*M* KBr, 5 m*M* $CuCl_2$ and 8 m*M* 2HP. Subsequently, data to 2.9 Å were collected as described above. All data was collected at beamline ID14-1, ESRF, Grenoble, France using an ADSC Q4 CCD detector. Data processing, integration and scaling were performed with *MOSFLM* v.6.2.4 (Leslie, 1992) and *SCALA* (Evans, 1997). Data-processing statistics are listed in Table 1.

2.3. Structure solution

The solution of the SSAO holoenzyme structure has been described in Jakobsson *et al.* (2005). Briefly, it was discovered that the crystals were twinned when the refinement of the initial solution obtained by molecular replacement in space group $P4_32_12$ stalled. Since the data also suffered from pseudo-symmetry and anisotropy, the twinning-analysis method developed by Padilla & Yeates (2003), which is insensitive to these phenomena, was used to estimate the twinning fraction. The data was detwinned with the program *DETWIN* (Taylor & Leslie, 1998) using different twinning fractions. Subsequently, the Padilla & Yeates method, as implemented in *DATAMAN* (Kleywegt & Jones, 1996*b*), was used to analyse the detwinned data sets. For the 3.0 Å data set, a twinning fraction of 0.25 yielded detwinned data that behaved like a non-twinned data set and that could be used to solve the structure by molecular replacement with *AMoRe* (Navaza, 1994). Data between 15 and 4.6 Å were used to obtain the solution in space group $P4_3$. A polyalanine model of the dimer of domain D4 (residues 231–646) of *P. sativum* CuAO (PDB code 1ksi; Kumar *et al.*, 1996) was used as the search model (the bovine and human models were not available at the time). The twinning fractions of the improved holoenzyme and 2HP adduct crystals were estimated in the same way to be 0.30 and 0.28, respectively. The structure of the inhibitor adduct was determined by isomorphous replacement using rigid-body refinement with *CNS* v.1.1 (Brünger *et al.*, 1998) of a polypeptide chain of the near-final model of the SSAO holoenzyme structure.

2.4. Structure refinement and rebuilding

The initial model of the holoenzyme was refined with *CNS* using simulated annealing and applying strong fourfold NCS restraints. The refinement rounds in *CNS* were alternated with manual rebuilding in *O* (Jones *et al.*, 1991). Density for one Cu^{2+}, two additional cations modelled as Ca^{2+} and one Cl^{-} per monomer was clearly visible at an early stage. Later, one additional Cl^{-} ion per monomer was added to the model. Water molecules were added using *CNS* and inspected in *O*. At five of the six putative N-glycosylation sites electron density for one or several sugar molecules was visible. Further refinement rounds were carried out with *REFMAC*5 (Murshudov *et al.*, 1997) using TLS with each molecule as a separate domain to a final *R* value of 0.204. The last recorded value of $R_{\rm free}$ (prior to the final refinement round against all data) was 0.252.

The initial model of the 2HP adduct was refined with *CNS* using simulated annealing and applying strong fourfold NCS restraints. Further refinement rounds in *CNS*, using the twin-refinement module, were alternated with manual rebuilding in *O* (Jones *et al.*, 1991) and twofold NCS restraints were used throughout the refinement. When one Cu^{2+}, two Ca^{2+} and one or two Cl^{-} per monomer had been added to the model, clear density near a number of histidines was observed. The 2HP soak contained 5 m*M* $CuCl_2$ and the density features were interpreted as six or seven additional Cu^{2+} ions per monomer. At four or five of the six putative N-glycosylation sites electron density for one or several sugar molecules was visible. The final *R* value was 0.211 and the last recorded value of $R_{\rm free}$ was 0.275.

Refinement and model statistics are listed in Table 2.

2.5. Model analysis

The models were validated using *O*, *OOPS*2 (Kleywegt & Jones, 1996*a*) and *WHAT IF* (Vriend, 1990). Superpositions of the structures were performed using *LSQMAN* (Kleywegt, 1996) and surface areas were calculated using *AREAIMOL* (Collaborative Computational Project, Number 4, 1994).

Energetically favourable interaction sites in the entrance funnel for an amine cation were calculated with the program *GRID* (v.22; Goodford, 1985). The region of interest was mapped to a grid of 27 × 37 × 31 Å centred on the cavity with a spacing of 0.5 Å. At every point of this grid, the energy of

Table 3
Comparison of the monomer models.

Listed are the r.m.s.d. values (Å) for all C^{α} atoms that could be modelled. The diagonal shows the r.m.s.d. values between corresponding monomers in the holoenzyme and the 2HP adduct structure. Values below the diagonal are r.m.s.d. values between the 2HP adduct monomers and values above the diagonal are r.m.s.d. values between the holoenzyme monomers.

	A	*B*	*C*	*D*
A	0.47	0.28	0.16	0.27
B	0.50	0.54	0.27	0.17
C	0.12	0.46	0.46	0.28
D	0.51	0.10	0.46	0.53

interaction with a chemical probe, in this case N3+ (sp^3 amine NH3 cation), was evaluated.

Disordered regions were predicted with the *PONDR* server (Li *et al.*, 1999; Molecular Kinetics, 2004).

3. Results

3.1. Structure determination

All our crystals of SSAO suffered from twinning, pseudo-symmetry and anisotropic diffraction, which initially complicated the structure determination. Once the twinning problem had been recognized and the data detwinned, the crystal structure of the human SSAO holoenzyme was solved by molecular-replacement methods as described previously (Jakobsson *et al.*, 2005). The structure of pea seedling CuAO was used as a search model since the bovine and human structures were not available at the time. A near-final model of our holoenzyme structure was used to solve the structure of the adduct with the irreversible inhibitor 2HP. Models of the holoenzyme structure and of the 2HP adduct have been refined to 2.5 and 2.9 Å, respectively. Final $R/R_{\rm free}$ values are 0.204/0.252 for the holoenzyme structure and 0.215/0.276 for the 2HP adduct structure.

Despite the problems with anisotropy, pseudo-symmetry, twinning and the limited resolution of the data, the electron density for the holoenzyme is of surprisingly good quality except for the N- and C-terminal region and around residues 203–205. The maps of the 2HP adduct are of poorer quality and side chains with inferior electron density have been modelled in analogy with the isomorphous holoenzyme structure. An overview of the data-processing statistics is given in Table 1 and refinement and validation statistics are listed in Table 2.

3.2. The structure of SSAO

There are two dimers in the asymmetric unit comprising monomers *A* and *B* and monomers *C* and *D*, respectively. As a consequence of the pseudo-symmetry of the crystals (Jakobsson *et al.*, 2005), the two homodimers are very similar even when refined without non-crystallographic symmetry restraints. Monomers *A* and *C* are essentially identical and so are *B* and *D* (Table 3). Hence, the corresponding residues to those visible in *A* and *B* are visible in molecule *C* and *D*, respectively. In the following, we therefore limit our description and discussion to the *A*/*B* dimers of the holoenzyme and adduct structures, but the same applies to the *C*/*D* dimer unless explicitly stated otherwise.

The holoenzyme structure comprises residues *A*41, *A*58–*A*761, *B*39–*B*43 and *B*58–*B*761. The N-terminus and the last two residues of the C-terminus are probably disordered as no density is observed for residues *A*29–*A*40, *A*42–*A*57, *A*762, *A*763, *B*29–*B*38, *B*44–*B*57, *B*762 and *B*763. One copper ion, two calcium ions and two chloride ions were modelled in each monomer. Carbohydrate chains were built at four N-glycosylation sites on the *A* and *C* molecules and at five sites on the *B* and *D* molecules. 563 water molecules were included in the model.

The structure of the 2HP adduct comprises residues *A*58–*A*728 and *B*58–*B*728. The N- and C-termini are probably disordered and no density is observed for residues 29–57 and 729–763 in any of the chains. The 2HP adduct of the TPQ cofactor has been modelled in the active site. A number of electron-density features near histidines were modelled as copper ions as $CuCl_2$ was part of the soaking solution. Altogether, seven or eight copper ions, two calcium ions and one or two chloride ions were modelled in each monomer. Carbohydrate molecules were built at four N-glycosylation sites on the *A* and *C* molecules and at five sites on the *B* and *D* molecules. 60 water molecules were included in the model.

The ordered parts of the holoenzyme and the 2HP adduct structures are very similar, with an r.m.s.d. of ∼0.5 Å for ∼670 C^{α} atoms when comparing corresponding monomers (Table 3). However, one of the additional copper ions changes the conformation of a hairpin loop that contains an RGD motif (residues 726–728) and residues 729–761 are not visible at all, unlike in the holoenzyme structure.

The overall structure of human SSAO (Fig. 1) is similar to that of the previously reported CuAOs. They all share a similar fold and contain three domains that are called D2, D3 and D4. The highest degree of structural similarity between these CuAOs is observed for the central D4 β-sandwich domain, which contains the dimer interface. On the outside of the D4 domain there are two smaller α/β-domains, D2 and D3. The first CuAO structure from *E. coli* was described as having the shape of a mushroom in which D2, D3 and D4 form the cap. In addition to these three domains, the *E. coli* protein contains a fourth domain, D1, that forms the stalk of the mushroom, and D1–D1 interactions contribute to the dimer interface (Parsons *et al.*, 1995).

In the human SSAO structure, domain D2 comprises residues 58–162. A nine-residue linker connects D2 with D3, which starts at residue 172 and continues to 283. Between D3 and D4 a linker consisting of residues 284–322 runs from the mushroom cap, along the side of the molecule near the dimer interface and towards the membrane side of the molecule where D4 starts. D4 contains the active site and is the largest domain, comprising residues 323–761. The interface between the two monomers in the dimer is composed of residues from domain D4 and buries ∼8700 $Å^2$ of the solvent-accessible surface area of each monomer. Two hairpin arms in each

monomer embrace the neighbouring molecule. These two hairpins include residues 423–468 and 536–569, respectively. The C-termini of the two monomers run antiparallel to each other along the membrane side of the molecule. There is no visible density for most of the 30 N-terminal residues, which form the linker to the putative membrane-spanning helix. However, persistent density was observed for some entity bound to Cys748 in D4. This was interpreted as a disulfide bridge between Cys41 and Cys748. The disulfide bridge links the N- and the C-terminus and the polypeptide thus forms a ring. The two rings in the dimer are interlocked, a topology that was also observed in the PPLO structure (Duff *et al.*, 2003).

In our construct, there are nine cysteines in each monomer and eight of these are involved in disulfide bridges. As described above, one of them links the N- and C-terminus (Cys41–Cys748). In another, two adjacent cysteines in domain D3, Cys198 and Cys199, form a vicinal disulfide bridge. This is a fairly uncommon structural feature that could play a structural role or be involved in electron exchange (Carugo *et al.*, 2003). The disulfide forces the backbone to make a sharp turn (distorted type I; Wilmot & Thornton, 1988). A stabilizing disulfide bridge between Cys404 and Cys430 is found in domain D4 and is present in all structures except ECAO. Finally, a small loop is created in the C-terminus by a bridge between Cys734 and Cys741. This probably helps to position and stabilize the hairpin loop (725–731), which exposes an RGD motif (Arg726, Gly727, Asp728) at its tip. The only unpaired cysteine residue (Cys95) is located in the β-sheet in domain D2, $\sim$10 Å from the active-site entrance

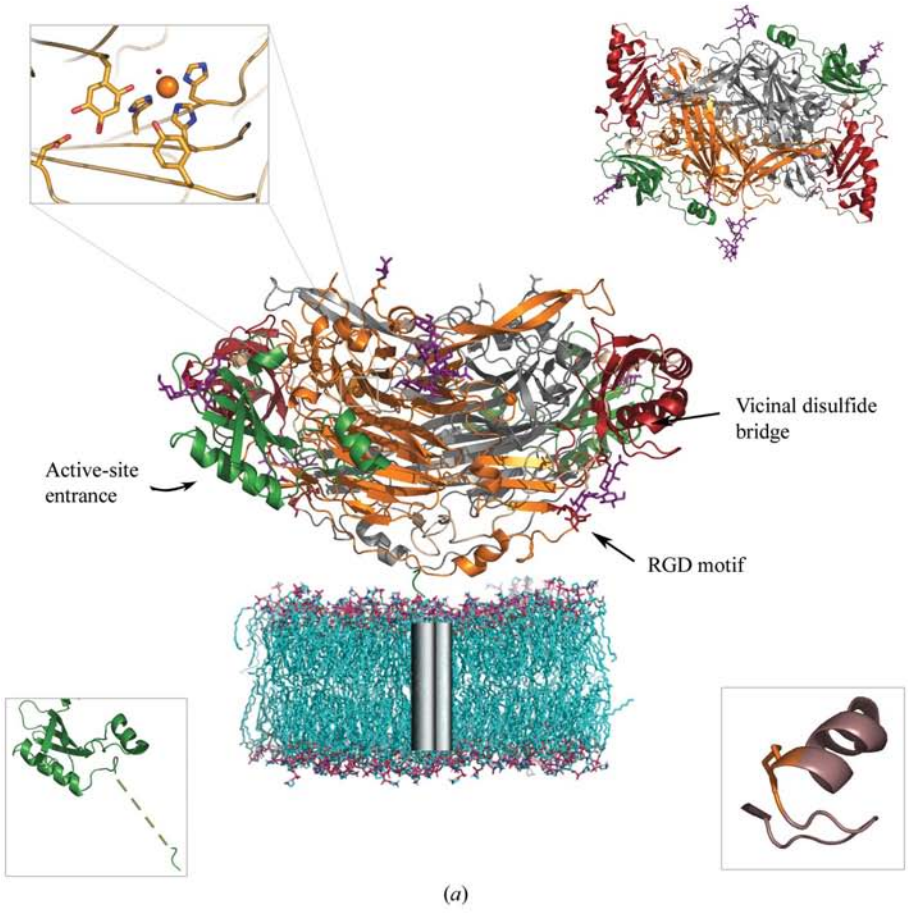

Figure 1
(*a*) Overview of the human SSAO structure. Domain D2 is shown in green, domain D3 in red and domain D4 in grey (monomer *A*) or orange (monomer *B*) and carbohydrates are shown as purple sticks. The lipid bilayer (Tieleman & Berendsen, 1998) is shown merely to illustrate the putative position of the molecule with respect to the membrane. The grey cylinders represent the membrane-bound helices. The insets show, clockwise from the top left, the active site of SSAO, a view of the homodimer from the top towards the membrane, the vicinal disulfide bridge and parts of domain D2 indicating the location of the non-observed residues 43–57. This figure, as well as Figs. 2, 3*b*, 4*b*, 5, 6, 7 and 8, was created with *PyMOL* (DeLano, 2002). (*b*) Topology of human SSAO. The residue numbers indicate the beginning and end of secondary-structure elements and the latter have been coloured as in (*a*). The positions of the TPQ, the histidine residues that coordinate the copper, disulfide bridges and the potential N-glycosylation sites are indicated.

funnel and ∼7 Å from the surface. The full-length protein contains one additional cysteine (Cys22), which is located in the putative N-terminal transmembrane helix.

There are six potential N-glycosylation sites on full-length SSAO, namely asparagines 137, 232, 294, 592, 618 and 666. At five of these sites electron density is visible for a carbohydrate moiety attached to the asparagines. We have not observed any evidence in the electron density for O-glycosylated serine or threonine residues.

3.3. The active site

The active site is located in domain D4 and includes the TPQ cofactor and the three conserved histidines, His520, His522 and His684, that coordinate the copper ion (Fig. 2). A conserved water molecule, W_a, acts as an axial copper ligand. In some structures an equatorial water, W_e, has also been observed (Brazeau *et al.*, 2004). However, this water is labile (Murray *et al.*, 1999) and is not visible in our density maps. Previous crystal structures have revealed that the TPQ cofactor is mobile and two extreme conformations have been observed. In the 'on-copper' conformation, TPQ is in direct contact with the copper *via* O4, whereas in the 'off-copper' conformation TPQ O2 forms a hydrogen bond to W_a. In our structure, O2 of TPQ points towards W_a in both subunits and the cofactor is thus in the active 'off-copper' position. In the previously described 'off-copper' structures, TPQ O4 forms a short hydrogen bond (∼2.4 Å) with the conserved Tyr372 OH and this interaction is thought to keep TPQ and the reaction intermediates in a favourable position during catalysis (Wilmot *et al.*, 1997; Mure, Kurtis *et al.*, 2005). In our structure the TPQ cofactor is tilted towards the substrate-binding pocket and the distance between Tyr372 OH and O4 is 5 Å in both monomers. Instead, the distances between TPQ O4/O5 and $O^{\delta1}/O^{\delta2}$ of Asp386, the catalytic base, are shorter (3–4 Å). However, as in most of the previous CuAO structures, the density for the cofactor is not entirely unambiguous (Fig. 2).

3.4. The 2HP adduct structure

Primary amines are the substrates of SSAO. 2HP belongs to a group of irreversible substrate-like CuAO inhibitors in which the α-methylene C atom has been replaced by nitrogen. This prevents completion of the reaction and thus prevents product release. The inhibitor reacts at the C5 position of the TPQ (Fig. 3*a*) cofactor and forms a hydrazone that is converted to an azo product at high pH (∼9–10) or by urea denaturation (Mure, Kurtis *et al.*, 2005). In the present study, the crystals were grown at pH 5 and the 2HP adduct is expected to exist predominantly as a hydrazone (Fig. 3*a*). Asp386, the presumed catalytic base, forms hydrogen bonds to N2 and N3, of which the interaction with N3 appears to be the strongest. A stacking interaction between Tyr384 and the pyridine ring further stabilizes the conformation of 2HP (Fig. 3*b*). In 2HP adducts with ECAO (Wilmot *et al.*, 1997; Mure, Brown *et al.*, 2005) a short hydrogen bond (2.3 Å) is observed between TPQ O4 and Tyr372, but in our structure the distance ranges between 3.4 and 3.8 Å in the various monomers. However, the density for the 2HP adduct is poor, probably owing to a combination of limited resolution, weak and incomplete data, problems with twinning and anisotropy, static or dynamic disorder and less than unit

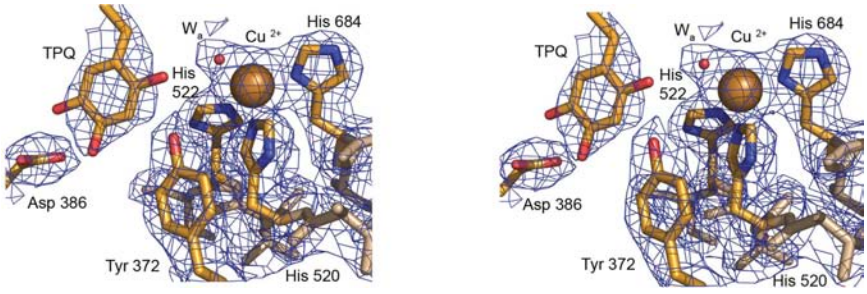

Figure 2
Stereoview of the active site of SSAO showing the TPQ cofactor, the copper site, Tyr372 and the active-site base Asp386. The σ_A-weighted $2mF_{obs} - DF_{calc}$ electron-density map is contoured at a level of 1.0σ.

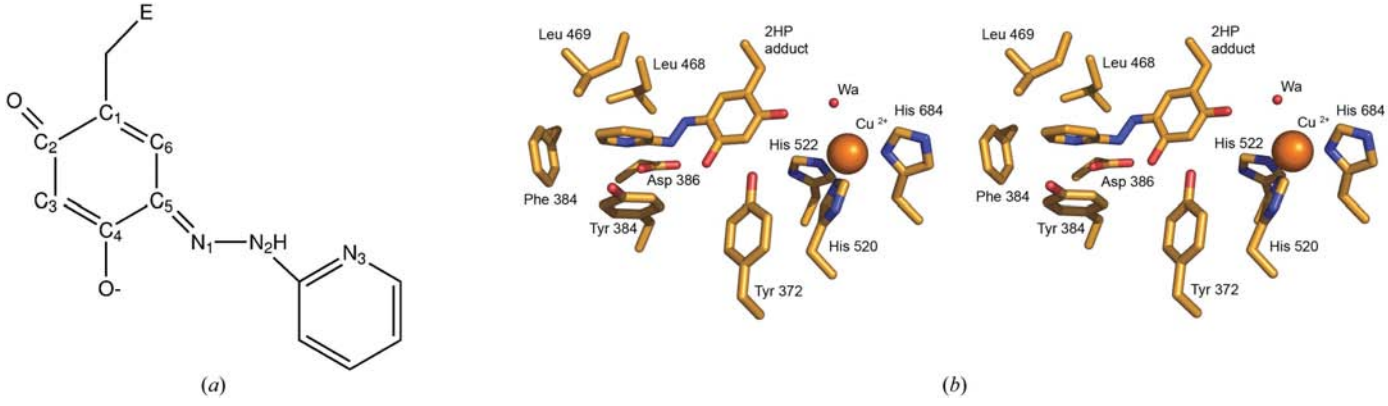

Figure 3
(*a*) Structure of the hydrazone form of the adduct of the TPQ cofactor and the irreversible inhibitor 2-hydrazinopyridine (2HP). E denotes the enzyme. The figure was created using *ChemDraw*. (*b*) Stereoview of the active site in the 2HP adduct structure.

occupancy of the reaction product. Nevertheless, the structure gives an indication of the conformation a substrate Schiff base could assume.

3.5. The entrance funnel to the active site and the 'lake'

A flattened funnel leads from the surface to the active site. As in BSAO and PPLO, the funnel is broad compared with that of other known CuAO structures and appears to be exposed to solvent. The wide-mouthed funnel is approximately 22 Å deep and the width and height at the entrance are around 25 and 8 Å, respectively. Residues in domains D3 and D4 and one of the arms from the other subunit form the surface of the funnel (Fig. 4*b*). Carbohydrates attached to Asn232 and the four last residues at the C-terminus (758–761) affect the size of the entrance. Density for a GlcNAc-GlcNAc moiety attached to Asn232 is visible in the holoenzyme structure, but the actual carbohydrate structure might be larger than this. The electron density for the C-terminus is poor, which suggests that this region might be flexible. There is no density at all for the two C-terminal residues (residues 762–763), which could further alter the appearance of the entrance.

The steep walls of the funnel are composed of residues 85–88 of domain D2, 173–184, 206–212 and 238–239 of domain D3, 389, 393–397, 415–426, 467–469 and 758–761 (and possibly the unobserved residues 762–763) of domain D4, 446–450 located on the arm from the other monomer and the carbohydrates attached to Asn232 (Fig. 4*b*). Many of the residues lining the funnel are aromatic or hydrophobic, but one of the corners in the flattened funnel contains two lysines, whereas the other corner includes a number of polar and negatively charged residues.

A cluster of energetically favourable binding sites for an amine ion (NH_3^+) is found on the walls of the funnel defined by residues in domain D4 near the surface and residues on domain D3 deeper in and closer to the active site (Fig. 4*a*). The favourable sites are mainly a consequence of backbone carbonyl O atoms but also of Asp446 of the neighbouring monomer. In the vicinity of the active site, both the TPQ cofactor and Asp386 attract the positive amine group.

A tyrosine close to TPQ has been proposed to act as an 'active-site gate' in all previous CuAO structures, except in HPAO where it is replaced by a much smaller alanine residue. The tyrosine at this position in SSAO, Tyr384, is positioned such that substrates can reach the active site. However, in SSAO as well as in BSAO, the accessibility of the active site is restricted by the presence of a leucine residue (Leu469; Fig. 5). As pointed out by Lunelli *et al.* (2005), other CuAO structures have a glycine at this position or, in the case of HPAO, an alanine. This leucine makes the gate narrower in SSAO and BSAO than in other CuAOs and reduces the accessibility of the active site from the entrance funnel. The conformation of this leucine is different in SSAO and BSAO, resulting in an even tighter entrance in SSAO. Further, the leucines in SSAO and BSAO, as well as the alanine in HPAO, are outliers in the Ramachandran plot. This implies that there is some strain in the backbone, which is often observed for functionally important residues (Herzberg & Moult, 1991).

A water-filled cavity between the subunits has been suggested to function as an inlet and outlet for small reagents and reaction products such as dioxygen, hydrogen peroxide and ammonia (Wilce *et al.*, 1997; Duff *et al.*, 2003; Lunelli *et al.*, 2005). As was observed in the structure of BSAO, a wide mouth at the surface connects the internal cavity to the external solvent through three small channels. However, whereas in BSAO the three channels are connected to one single cavity (the 'lake'), they are confluent in SSAO (Fig. 6). This is owing to differences in the position of residues Gly698 and Asn699. In SSAO, this results in one larger central cavity and two channels, one on each side. These minor channels are connected to the copper site and have His684 as one of the bounding residues.

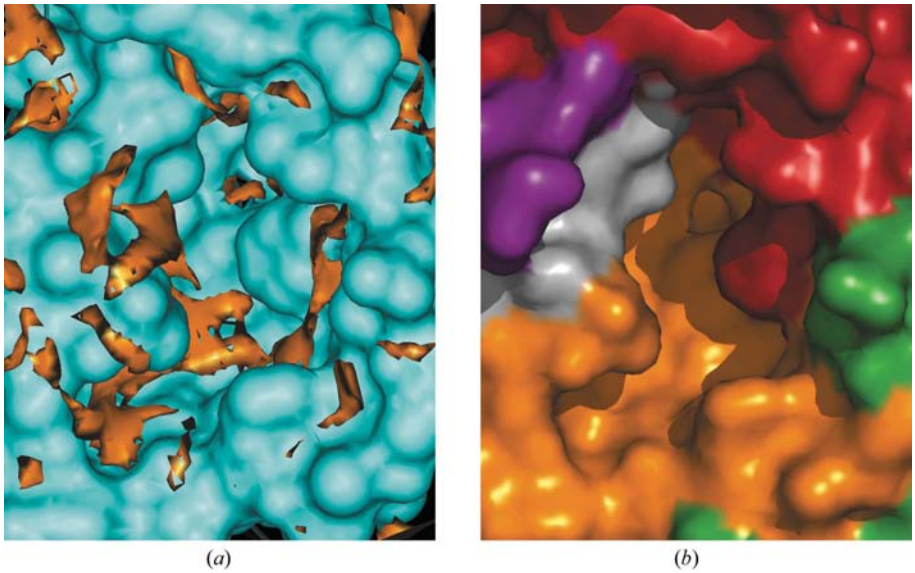

Figure 4
Close-up view of the flattened funnel that leads to the active site. (*a*) Energetically favourable interaction regions for an amine cation in the entrace funnel were calculated using the program *GRID* (Goodford, 1985). The isocontour at -33 kJ mol^{-1} is shown in orange and the surface of the protein in cyan. The figure was created using *Insight II* (Accelrys). (*b*) The surface of the funnel, using the same colour scheme as in Fig. 1(*a*).

3.6. Amino-acid composition

Human SSAO contains few lysines (1.8% compared with 5.4% on average for proteins in the Uniref50 database) and rather many prolines (7.9% compared with 5.2%) and the numbers are similar for BSAO. Comparisons with ECAO, AGAO, HPAO, PSAO and PPLO show that AGAO has a similarly low lysine content, albeit compensated by a large number of arginines, and all

except PPLO have a high proline content. This observation is somewhat intriguing since lysine residues are potential substrates of SSAO. Andrade *et al.* (1998) compared the amino-acid composition on the surface of nuclear, cytoplasmic and extracellular proteins and found that extracellular proteins in general have a lower number of charged residues on the surface and in particular the lysine content was reduced compared with cytoplasmic and nuclear proteins. All compared CuAOs have an excess of acidic residues, ranging from a surplus of nine (HPAO) to 59 (PPLO). For SSAO and BSAO the surplus is 14 and 21, respectively. However, SSAO is a sialoglycosylated protein and the charged carbohydrate moieties will also affect the electrostatic character of the surface. Many of the prolines are found in the linker between domains D3 and D4 and near the C-terminus. These stretches are located on the membrane side of D4, have relatively high temperature factors (especially the C-terminus) and are predicted to be disordered by the *PONDR* server (Li *et al.*, 1999). In addition to these regions, residues 29–48, 107–117, 144–149 and 635–648 are predicted to be disordered regions. No density is observed for residues 29–38 and 43–57. The remaining three stretches have relatively high temperature factors and surround a cavity at the top of the mushroom between domains D2 and D4. The entrance to this cavity is lined with negatively charged residues (Glu158, Glu634 and Glu640) and the area is encircled by the carbohydrates attached to Asn137, Asn592 and Asn666.

3.7. Comparison with related structures

As expected, the overall structure of human SSAO is very similar to that of BSAO (r.m.s.d. 0.7 Å for 623 pairs of C^{α} atoms). However, some regions that were not built in the BSAO model could be modelled for human SSAO. These include residues 293–321 and 718–762 (corresponding to 294–322 and 717–761, respectively, in human SSAO). The fragment from 293–321 is the linker between domains D3 and D4 that runs along the side of the molecule near the dimer interface. The C-terminal stretch from 717–761 in human SSAO resembles the C-terminus in PPLO but is not observed in the other structures.

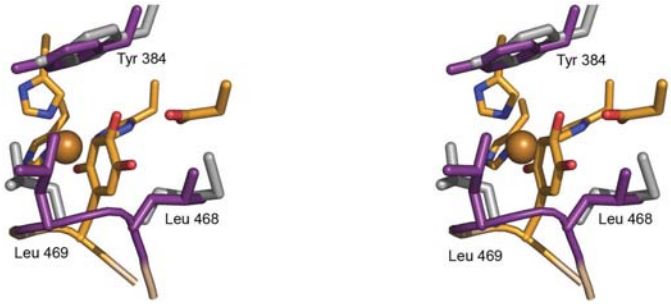

Figure 5
Stereoview of the narrow entrance to the active site. The end of the funnel is delimited by Tyr384, Leu468 and Leu469 in SSAO (purple), which correspond to Tyr383, Met467 and Leu468 in BSAO (grey; Lunelli *et al.*, 2005).

There are also several noticeable differences between human SSAO and BSAO. For instance, residues 202–207 (201–206 in BSAO) have been built differently in SSAO and BSAO (maximum $C^{\alpha}-C^{\alpha}$ distance 12 Å). However, the poor density suggests that this region is likely to be flexible.

A number of striking differences between SSAO and BSAO are found in the entrance and funnel to the active site. The tip of the arm from the neighbouring monomer located at the entrance to the active site (residues 446–452) has a different conformation in human SSAO owing to the carbohydrates attached to Asn232 and the proximity of residues 725–727 in the C-terminus (which were not observed in BSAO). The presence of the C-terminus, the carbohydrates and the different conformation of this loop result in a part of the entrance being blocked in SSAO, whereas it is unobstructed in BSAO. At the opposite side at the brim of the funnel, Leu172 in BSAO is replaced by Phe173 in SSAO and, further in, Tyr392 is replaced by Arg393, Phe393 by Tyr394 and Asn211 by Thr212. The available space just before the spout of the funnel is smaller in SSAO as Pro237-Tyr238 have been replaced by Phe238-Phe239. In the end of the funnel, Met467 was identified in BSAO as one of the delimiting residues

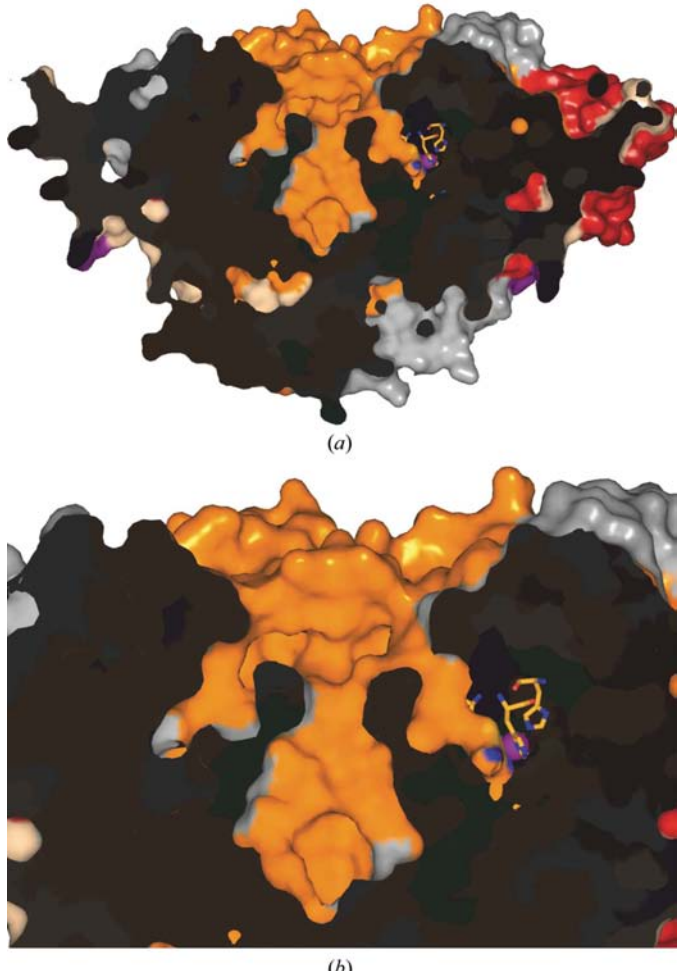

Figure 6
The lake in SSAO. (*a*) A cavity is formed between the two D4 domains in the homodimer. (*b*) Close-up view. The cavity divides into three separate voids and the side channels are in contact with the copper-binding site.

(Lunelli *et al.*, 2005) and the corresponding residue in SSAO is Leu468. Together with Leu469 (Leu468 in BSAO), which has a different conformation in SSAO than in BSAO, this pair of leucines makes the last part of the funnel narrower in SSAO compared with BSAO.

Finally, residues Gly698 and Asn699 between the copper-binding site and the large water-filled cavity or 'lake' point into the lake in the BSAO structure, whereas they point towards the active site in the human structure.

While this manuscript was in preparation, two human SSAO models were released by the PDB with codes 1pu4 and 1us1. Both structures were solved in space group $P6_522$ with similar unit-cell parameters and they were refined to 3.2 and 2.9 Å, respectively. Comparison of our model with 1us1 reveals that the modes are very similar (r.m.s.d. of ∼0.5 Å for ∼699 residues). However, there are some interesting differences. In our structure, a disulfide was modelled between Cys41 and Cys748. In 1us1 there is a disulfide bridge between the two monomers instead, linking *A*748 and *B*748. Furthermore, the TPQ cofactor is in the 'on-copper' conformation in 1us1, whereas it is in the 'off-copper' conformation in our structure. Residues 55–57 (GQS), which are not visible in our structure, have been modelled in 1us1. Both in our structure and in 1us1 there is poor electron density for the stretch 202–205 and it has been built differently in the two models. Finally, differences in the backbone are also found between residues 744 and 750.

4. Discussion

4.1. Active site

The make-up of the active-site entrance is important for substrate specificity in CuAOs. In SSAO, as in BSAO and PPLO, the entrance is a flattened and wide-mouthed funnel. Hydrophobic and aromatic residues dominate its walls, but some charged residues are found in the corners of the mouth. Favourable binding sites for a positively charged amine ion are found in the corner of the mouth near the entrance that is lined by residues from domain D4 (Fig. 4). Further in, however, there are additional binding sites on the walls demarcated by D3. In the end of the funnel, a leucine residue (Leu469) obstructs access to the active site (Fig. 5). This residue is also a leucine in BSAO, but there it has a different conformation which makes the opening larger. In all other CuAO structures, this residue is a glycine, except in HPAO, where it is an alanine. Although the density is clear for this residue in our structure, Leu469 could well be an additional 'active-site gate' that controls accessibility of the active site. The size of the mouth, and thus the accessibility of the funnel, is influenced by the carbohydrates attached to Asn232 and by the C-terminus.

The structure of the 2HP adduct was solved and the adduct was modelled as a hydrazone that resembles the substrate Schiff base. However, whereas the catalytic base Asp386 is deprotonated in the interaction with the substrate Schiff base, it is protonated in the interaction with the 2HP adduct (Mure, Brown *et al.*, 2005). In addition, whereas the substrate Schiff base is neutral, the 2HP adduct is monoanionic (Mure, Brown *et al.*, 2005). The N2 and N3 atoms of the adduct interact with the catalytic base, Asp386, and since N3 has no H atom attached to it (Fig. 3*a*), this indicates that the aspartate is indeed protonated ($O^{\delta1}$—N3 $\simeq$ 2.5 Å). The pyridine ring of the adduct stacks with Tyr384 in a hydrophobic pocket adjacent to the active site. Although the structure provides a useful model for the substrate Schiff base, the limited resolution and poor density for the 2HP moiety preclude more detailed conclusions.

4.2. Substrates and inhibitors

The identification of the physiological substrate(s) of SSAO is of great interest. Methylamine and aminoacetone have been put forward as plausible candidates (Lyles, 1996; Yu *et al.*, 2003; O'Sullivan *et al.*, 2004) and so have free amino groups on proteins and amino sugars (Salmi *et al.*, 2001; Göktürk, Nilsson *et al.*, 2003; Koskinen *et al.*, 2004; Sibon *et al.*, 2004). As the entrance funnel is spacious, it can hold relatively large substrates and can probably accommodate a lysine-exposing peptide. Lysine-containing peptides have been shown to inhibit SSAO/VAP-1-dependent lymphocyte rolling (Yegutkin *et al.*, 2004), but further experiments are needed to identify physiological substrate sequences. The present holoenzyme structure can be used for docking experiments and, in combination with structural studies of complexes and biochemical experiments, might give clues about the nature of the physiological substrate. Furthermore, development of specific SSAO inhibitors is desirable as they have potential as anti-inflammatory drugs (Merinen *et al.*, 2005; Stolen *et al.*, 2005; Vainio *et al.*, 2005) and they might also be able to alleviate some of the complications associated with diabetes (Ekblom, 1998). The structure of the 2-hydrazinopyridine adduct has also been determined. This adduct is analogous to the substrate Schiff-base reaction intermediate in its hydrazone form (presumed to be predominant in the crystal) and information about the active site in this structure might be useful in the inhibitor-design process.

Benzylamine is a good non-physiological substrate for SSAO as well as for another monoamine oxidase, namely the flavoprotein monoamine oxidase B (MAO B; Kinemuchi *et al.*, 2004), which means that the two proteins have an overlap in substrate specificity and this has to be considered in the development of inhibitors binding specifically to SSAO. The structures of both SSAO and MAO B (PDB code 1gos; Binda *et al.*, 2001) are now available and comparisons of the make-up of their respective active sites can be used to aid the development of specific inhibitors.

4.3. Dioxygen-binding sites

The location of the binding site(s) for dioxygen in the biogenesis of TPQ and the oxidative half-reaction is still unknown. Kinetic data suggests that no metal ions are involved in dioxygen binding (DuBois & Klinman, 2005). Instead, spectroscopic, kinetic and structural studies on HPAO by Klinman and coworkers implicate Met634 (corresponding

Table 4
Residues lining the xenon-binding sites found in AGAO, PPLO and PSAO (Duff *et al.*, 2003) and BSAO (Lunelli *et al.*, 2005) and the corresponding residues in ECAO, HPAO and SSAO.

Columns 1–6 refer to the Xe-binding site found in AGAO, PPLO, PSAO and BSAO, and columns 7–9 refer to the Xe-binding site found in BSAO that is in agreement with the site suggested in HPAO (DuBois & Klinman, 2005).

	1	2	3	4	5	6	7	8	9
ECAO	Ala484	Ala486	Tyr528	Thr687	Glu702	Val704	Tyr468	Ala486	Met699
HPAO	Ile423	Leu425	Phe460	Ile622	Glu637	Ile639	Tyr407	Leu425	Met634
PSAO	Ile405	Leu407	Tyr446	Ile601	Leu616	Thr618	Tyr389	Leu407	Met613
PPLO	Val496	Ala498	Leu532	Leu692	Ala709	Ala711	Tyr480	Ala498	Thr704
AGAO	Ala400	Ala402	Phe435	Leu590	Asp605	Val607	Tyr384	Ala402	Met602
BSAO	Leu488	Ala490	Ala523	Phe681	—	Val700	Tyr472	Ala490	Thr693
SSAO	Phe489	Ala491	Ala524	Phe682	Asn699	Val701	Tyr473	Ala491	Thr694

to Thr694 in SSAO) as a dioxygen-binding residue (DuBois & Klinman, 2005). Other studies have used xenon as a probe to detect hydrophobic cavities with the potential to bind dioxygen. One cavity in the vicinity of the active site was found to bind xenon in AGAO, PPLO and PSAO (Duff *et al.*, 2004). Xenon has also been found to bind in the same area in BSAO (Lunelli *et al.*, 2005), but unfortunately the coordinates for the sites in BSAO are not available. This common cavity is demarcated by Phe489, Ala491, Ala524, Phe682, Asn699 and Val701 in SSAO (Table 4) and is situated adjacent to the 'lake'. The cavity is mainly lined by hydrophobic and one or two aromatic residues in all structures (Table 4) and the charged residues that are found in some structures do not point into the cavity. Thus, the hydrophobic character of this cavity is conserved also in SSAO and it could potentially be a dioxygen-binding site. However, a xenon site with lower occupancy was also found between the TPQ and the copper site near Thr693 in BSAO (Lunelli *et al.*, 2005), which corresponds to Met634 in HPAO. This site is lined by Tyr472, Ala490 and Thr693 in BSAO and the corresponding residues in other structures are listed in Table 4. Structural studies of ECAO have indicated the presence of a binding site for dioxygen between the protonated O2 of the cofactor and the copper ion (Wilmot *et al.*, 1999).

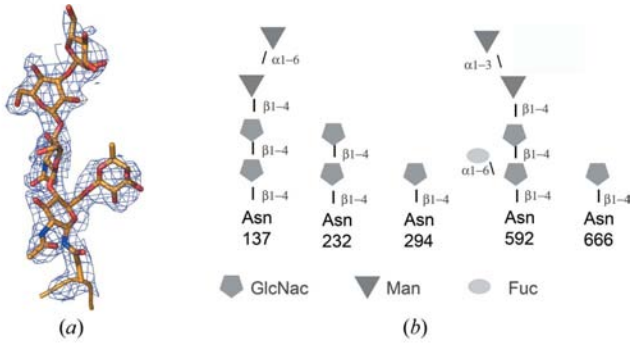

Figure 7
Experimentally observed N-glycosylation of SSAO. (*a*) σ_A-Weighted ($2mF_{obs} - DF_{calc}$) density, contoured at a level of 1.0σ, for Asn592 and the attached carbohydrate moieties in the *D* monomer. (*b*) Overview of the carbohydrate moieties modelled at the various N-glycosylation sites in monomer *D*. Abbreviations used: GlcNac, *N*-acetyl D-glucosamine; Man, D-mannose; Fuc, L-fucose.

4.4. Glycosylation

Sialylated carbohydrate decorations on the surface of SSAO are a prerequisite for lymphocyte binding (Salmi & Jalkanen, 1996) and five out of six potential N-glycosylation sites have density for one or several attached carbohydrate moieties (Figs. 1 and 7). Asn137 is positioned on the brim of the mushroom cap in D2 and Asn232 and Asn294 are located under the cap below domain D3. The active-site entrance is lined by sugars attached to Asn232. Asn592 and Asn666 are found in D4 on the top of the mushroom cap. There is no clear density for any sugar attached to Asn618, but it is located on the surface at the top of the mushroom-shaped molecule and could also be a glycosylation site.

4.5. Disulfides

SSAO contains four disulfide bridges in the holoenzyme structure: a vicinal bridge from Cys198 to Cys199 (Fig. 1*a*), a stabilizing bridge from Cys404 to Cys430 observed in all

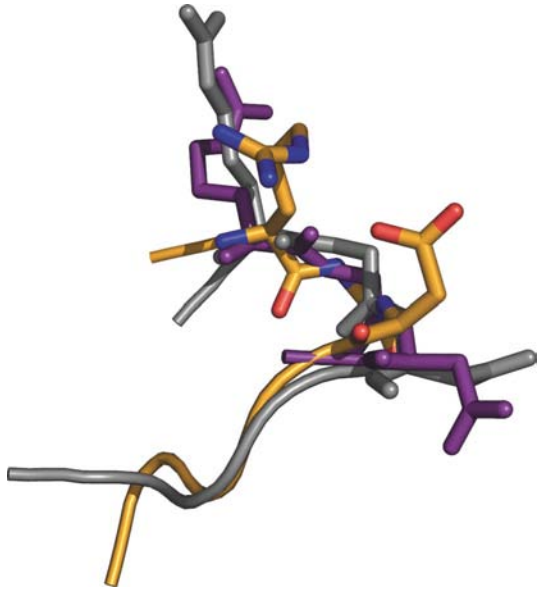

Figure 8
Comparison of the conformation of the RGD motif in SSAO with the RGD motif present in trimestatin (shown in grey; PDB code 1j2l; Fujii *et al.*, 2003) and the RGD-containing pentapeptide crystallized in complex with integrin $\alpha V\beta 3$ (shown in purple; PDB code 1l5g; Xiong *et al.*, 2002).

structures except ECAO, a loop-forming bridge between Cys734 and Cys741 (which helps orient the hairpin loop containing the RGD motif; Fig. 8) and the bridge that links the N- and C-terminus (Cys41–Cys748). In PDB entry 1us1, the latter form a link between the C-termini of the two monomers (Cys*A*748 and Cys*B*748). However, whereas 1us1 contains the full-length protein, we used a truncated form (residues 29–763). Hence, the disulfide bridge we observe between Cys41 and Cys748 could be an artefact of our protein-production protocol. If Cys748 forms a link between the two monomers in the full-length protein, this leaves Cys22 and Cys41 in both monomers that could form additional disulfide bridges. However, Cys22 is located in the putative transmembrane helix. Thus, in the full-length protein Cys41 of both monomers could form an additional inter-chain disulfide. Since soluble SSAO is derived from the membrane-bound form through proteolytic cleavage ('shedding'), it is likely that SSAO contains a protease cleavage site in the linker between the transmembrane helix and domain D2 (residues 28–58). A disulfide pairing of Cys41 from both monomers might help to fix or properly expose such a site.

4.6. A redox switch in SSAO?

Cysteine residues with lowered pK_a values can be oxidized by hydrogen peroxide (Rhee *et al.*, 2003). If these cysteine residues are vulnerable to oxidation by hydrogen peroxide in their reduced form, this could be part of a redox switch controlling conformational changes at the surface of the protein. SSAO activity is known to be required for the transmigration step in leukocyte extravasation (Koskinen *et al.*, 2004) and stimulates glucose uptake in adipocytes (Zorzano *et al.*, 2003). Hydrogen peroxide is one of the products of the SSAO-catalyzed reaction and since catalase abolishes the effect of SSAO activity on glucose uptake in adipocytes, hydrogen peroxide has been suggested to play a role in the mechanism (Zorzano *et al.*, 2003). In the light of these observations, it is tempting to speculate that conformational changes on the surface of SSAO induced by its product hydrogen peroxide could actually play an important role in this protein's mechanism of action. The most likely candidate to be involved in such a switch is the bridge from Cys198 to Cys199 as it is known that vicinal disulfide bridges can be involved in redox-switch mechanisms (Carugo *et al.*, 2003). Reduction of this bridge is likely to alter the shape of the protein surface in the vicinity of the active-site entrance. Clearly, testing of this hypothesis requires further experiments, involving mutations of these two cysteine residues.

4.7. RGD motif

SSAO contains the classic integrin-binding sequence RGD (Rouslahti, 1996) at residues 726–728, which are found at the surface of the protein in the vicinity of the active-site entrance. The motif is presented on the tip of a hairpin loop whose conformation resembles that found in trimestatin (Fujii *et al.*, 2003), an integrin-binding protein found in snake venom, as well as the conformation of the RGD motif in a pentapeptide crystallized in complex with integrin $\alpha V\beta 3$ (Xiong *et al.*, 2002; Fig. 8). However, the significance of this motif in SSAO is not yet known. It could be involved in integrin-mediated cell attachment, but neither alterations in this sequence nor pre-treatment of lymphocytes with a peptide containing the RGD motif abolished lymphocyte adhesion, although complete deletion diminished the binding (Salmi *et al.*, 2000).

The source of the soluble enzyme circulating in the bloodstream is thought to be membrane-bound SSAO that is released into the blood stream by a metalloprotease (Göktürk, Nilsson *et al.*, 2003; Abella *et al.*, 2004; Stolen *et al.*, 2004). ADAMs (an abbreviation for 'a disintegrin and metalloprotease') are a family of multi-domain proteins that contain a metalloprotease domain, that are involved in ectodomain shedding and that contain an integrin-binding motif (Bridges & Bowditch, 2005). It is thought that integrins could target ADAMs to the substrate protein. Hence, by analogy, it is possible that the RGD motif might be involved in the release of membrane-bound SSAO into the bloodstream by recruiting an integrin with the RGD motif, which in turn could recruit an ADAM protein. If our assumption of a disulfide bridge between Cys*A*41 and Cys*B*41 is correct, a protease-cleavage site is likely to be located between residues 28 and 58. On the other hand, if the intra-monomer pairing (48–748) observed in our structure is also the native pairing, the cleavage site would most probably be located between residues 28 and 41 (sequence RGGDGGEPSQLPHC). Such a site could in principle also be located in the transmembrane helix, but this is less likely as shedding often requires access to an unobstructed or flexible loop of sufficient length (Schwager *et al.*, 2001). However, very little is known at present about consensus cleavage sequences of ADAM proteins (Cheng *et al.*, 2003). This hypothesis, too, could be tested by examining the effect of mutations in the RGD motif on the shedding of SSAO.

Note added in proof: while this manuscript was being finalized for submission, a paper describing the structure of full-length SSAO/VAP-1 was published (Airenne *et al.*, 2005). Overall, the structures of the holoenzyme are very similar. The authors of that paper also noted the possible role of Leu469, the solvent-exposed RGD motif and the N-glycosylation sites. However, in the present manuscript the active 'off-copper' conformation is described, whereas the inactive 'on-copper' conformation was described by Airenne and coworkers.

We wish to thank Dr Martin Norin (Biovitrum), who initiated the collaboration between the two laboratories, Ulla Källström (Biovitrum) for expression of the protein, Hugo Gutiérrez de Teran (Uppsala University) for help with the *GRID* calculations, Nancy Fehrman of the high-throughput crystallization laboratory at the Hauptman–Woodward Institute in Buffalo (NY) for help with crystal-growth screening and the staff at beamline ID14-1 at the European Synchrotron Radiation Facility (ESRF), Grenoble (France) for help with data collection. EJ was supported in part through a grant from

the Swedish Structural Biology Network (SBNet) to GJK. GJK is a Royal Swedish Academy of Sciences (KVA) Research Fellow supported through a grant from the Knut and Alice Wallenberg Foundation.

References

Abella, A., Garcia-Vicente, S., Viguerie, N., Ros-Baro, A., Camps, M., Palacin, M., Zorzano, A. & Marti, L. (2004). *Diabetologia*, **47**, 429–438.

Airenne, T. T., Nymalm, Y., Kidron, H., Smith, D. J., Pihlavisto, M., Salmi, M., Jalkanen, S., Johnson, M. S. & Salminen, T. A. (2005). *Protein Sci.* **14**, 1964–1974.

Andrade, M. A., O'Donoghue, S. I. & Rost, B. (1998). *J. Mol. Biol.* **276**, 517–525.

Binda, C., Newton-Vison, P., Hubálek, F., Edmondson, D. E. & Mattevi, A. (2001). *Nature Struct. Biol.* **9**, 22–26.

Boomsma, F., Bhaggoe, U. M., van der Houwen, A. M. B. & van den Meiracker, A. H. (2003). *Biochim. Biophys. Acta*, **1647**, 48–54.

Brazeau, B. J., Johnson, B. J. & Wilmot, C. M. (2004). *Arch. Biochem. Biophys.* **428**, 22–31.

Bridges, L. C. & Bowditch, R. D. (2005). *Curr. Pharmaceut. Des.* **11**, 837–847.

Brünger, A. T., Adams, P. D., Clore, G. M., DeLano, W. L., Gros, P., Grosse-Kunstleve, R. W., Jiang, J.-S., Kuszewski, J., Nilges, M., Pannu, N. S., Read, R. J., Rice, L. M., Simonson, T. & Warren, G. L. (1998). *Acta Cryst.* D**54**, 905–921.

Carugo, O., Cemazar, M., Zahariev, S., Hudaky, I., Gaspari, Z., Perczel, A. & Pongor, S. (2003). *Protein Eng.* **16**, 637–639.

Cheng, Q.-C., Tikhomirov, O., Zhou, W. & Carpenter, G. (2003). *J. Biol. Chem.* **278**, 38421–38427.

Collaborative Computational Project, Number 4 (1994). *Acta Cryst.* D**50**, 760–763.

DeLano, W. L. (2002). *PyMOL*. DeLano Scientific, San Carlos, CA, USA. http://www.pymol.org.

DuBois, J. L. & Klinman, J. P. (2005). *Arch. Biochem. Biophys.* **433**, 255–265.

Duff, A. P., Cohen, A. E., Ellis, P. J., Kuchar, J. A., Langley, D. B., Shepard, E. M., Dooley, D. M., Freeman, H. C. & Guss, J. M. (2003). *Biochemistry*, **42**, 15148–15157.

Duff, A. P., Trambaiolo, D. M., Cohen, A. E., Ellis, P. J., Juda, G. A., Shepard, E. M., Langley, D. B., Dooley, D. M., Freeman, H. C. & Guss, J. M. (2004). *J. Mol. Biol.* **344**, 599–607.

Engh, R. A. & Huber, R. (1991). *Acta Cryst.* A**47**, 392–400.

Ekblom, J. (1998). *Pharmacol. Res.* **37**, 87–92.

Evans, P. R. (1997). *Jnt CCP4/ESF–EAMCB Newsl. Protein Crystallogr.* **33**, 22–24.

Fujii, Y., Okuda, D., Fujimoto, Z., Horii, K., Morita, T. & Mizuno, H. (2003). *J. Mol. Biol.* **332**, 1115–1122.

Göktürk, C., Garpenstrand, H., Nilsson, J., Nordquist, J., Oreland, L. & Forsberg-Nilsson, K. (2003). *Biochim. Biophys. Acta*, **1647**, 88–91.

Göktürk, C., Nilsson, J., Nordquist, J., Kristensson, M., Svensson, K., Söderberg, C., Israelson, M., Garpenstrand, H., Sjöquist, M., Oreland, L. & Forsberg-Nilsson, K. (2003). *Am. J. Pathol.* **163**, 1921–1928.

Goodford, P. J. (1985). *J. Med. Chem.* **28**, 849–857.

Herzberg, O. & Moult, J. (1991). *Proteins*, **11**, 223–229.

Jakobsson, E., Nilsson, J., Källström, U., Ogg, D. & Kleywegt, G. J. (2005). *Acta Cryst.* F**61**, 274–278.

Jalkanen, S. & Salmi, M. (2001). *EMBO J.* **20**, 3893–3901.

Janes, S. M., Mu, D., Wemmer, D., Smith, A. J., Kaur, S., Maltby, D., Burlingame, A. L. & Klinman, J. P. (1990). *Science*, **248**, 981–987.

Jones, T. A., Zou, J. Y., Cowan, S. W. & Kjeldgaard, M. (1991). *Acta Cryst.* A**47**, 110–119.

Karádi, I., Mészáros, Z., Csányi, A., Szombathy, T., Hosszúfalusi, N., Romics, L. & Magyar, K. (2002). *Clin. Chim. Acta*, **323**, 139–146.

Kinemuchi, H., Sugimoto, H., Obata, T., Satoh, N. & Ueda, S. (2004). *Neurotoxicology*, **25**, 325–335.

Kleywegt, G. J. (1996). *Acta Cryst.* D**52**, 842–857.

Kleywegt, G. J. & Jones, T. A. (1996*a*). *Acta Cryst.* D**52**, 829–832.

Kleywegt, G. J. & Jones, T. A. (1996*b*). *Structure*, **4**, 1395–1400.

Klinman, J. P. (2003). *Biochim. Biophys. Acta*, **1647**, 131–137.

Koskinen, K., Vainio, P. J., Smith, D. J., Pihlavisto, M., Ylä-Herttuala, S., Jalkanen, S. & Salmi, M. (2004). *Blood*, **103**, 3388–3395.

Kumar, V., Dooley, D. M., Freeman, H. C., Guss, J. M., Harvey, I., McGuirl, M. A., Wilce, M. C. & Zubak, V. M. (1996). *Structure*, **4**, 943–955.

Langford, S. D., Trent, M. B., Balakumaran, A. & Boor, P. J. (1999). *Toxicol. Appl. Pharmacol.* **155**, 237–244.

Leslie, A. G. W. (1992). *Jnt CCP4/ESF–EACBM Newsl. Protein Crystallogr.* **26**.

Li, R., Klinman, J. P. & Mathews, F. S. (1998). *Structure*, **6**, 293–307.

Li, X., Romero, P., Rani, M., Dunker, A. K & Obradovic, Z. (1999). *Genome Inform.* **10**, 30–40.

Luft, J. R., Collins, R. J., Fehrman, N. A., Lauricella, A. M., Veatch, C. K. & DeTitta, G. T. (2003). *J. Struct. Biol.* **142**, 170–179.

Lunelli, M., Di Paolo, M. L., Biadene, M., Calderone, V., Battistutta, R., Scarpa, M., Rigo, A. & Zanotti, G. (2005). *J. Mol. Biol.* **346**, 991–1004.

Lyles, G. A. (1996). *Int. J. Biochem. Cell Biol.* **28**, 259–274.

Matthews, B. W. (1968). *J. Mol. Biol.* **33**, 491–497.

Merinen, M., Irjala, H., Salmi, M., Jaakkola, I., Hänninen, A. & Jalkanen, S. (2005). *Am. J. Pathol.* **166**, 793–800.

Molecular Kinetics Inc. (2004). *PONDR. Predictors of Natural Disordered Regions*. Molecular Kinetics Inc., Indianapolis, IN USA. http://www.pondr.com.

Mure, M., Brown, D. E., Saysell, C., Rogers, M. S., Wilmot, C. M., Kurtis, C. R., McPherson, M. J., Phillips, S. E. V., Knowles, P. F. & Dooley, D. M. (2005). *Biochemistry*, **44**, 1568–1582.

Mure, M., Kurtis, C. R., Brown, D. E., Rogers, M. S., Tambyrajah, W. S., Saysell, C., Wilmot, C. M., Phillips, S. E. V., Knowles, P. F., Dooley, D. M. & McPherson, M. J. (2005). *Biochemistry*, **44**, 1583–1594.

Mure, M., Mills, S. A. & Klinman, J. P. (2002). *Biochemistry*, **41**, 9269–9278.

Murray, J. M., Saysell, C. G., Wilmot, C. M., Tambyrajah, W. S., Jaeger, J., Knowles, P. F., Phillips, S. E. V. & McPherson, M. J. (1999). *Biochemistry*, **38**, 8217–8227.

Murshudov, G. N., Vagin, A. A. & Dodson, E. J. (1997). *Acta Cryst.* D**53**, 240–255.

Navaza, J. (1994). *Acta Cryst.* A**50**, 157–163.

Nymalm, Y., Kidron, H., Soderholm, A., Viitanen, L., Kaukonen, K., Pihlavisto, M., Smith, D., Veromaa, T., Airenne, T. T., Johnson, M. S. & Salminen, T. A. (2003). *Acta Cryst.* D**59**, 1288–1290.

O'Sullivan, J., Unzeta, M., Healy, J., O'Sullivan, M. I., Davey, G. & Tipton, K. F. (2004). *Neurotoxicology*, **25**, 303–315.

Padilla, J. E. & Yeates, T. O. (2003). *Acta Cryst.* D**59**, 1124–1130.

Parsons, M. R., Convery, M. A., Wilmot, C. M., Yadav, K. D., Blakeley, V., Corner, A. S., Phillips, S. E., McPherson, M. J. & Knowles, P. F. (1995). *Structure*, **3**, 1171–1184.

Rhee, S. G., Chang, T.-S., Bae, Y. S., Lee, S.-R. & Kang, S. W. (2003). *J. Am. Soc. Nephrol.* **14**, S211–S215.

Rouslahti, E. (1996). *Annu. Rev. Cell. Dev. Biol.* **12**, 697–715.

Salmi, M. & Jalkanen, S. (1996). *J. Exp. Med.* **183**, 569–579.

Salmi, M. & Jalkanen, S. (2001). *Trends Immunol.* **22**, 211–216.

Salmi, M., Stolen, C., Jousilahti, P., Yegutkin, G. G., Tapanainen, P., Janatuinen, T., Knip, M., Jalkanen, S. & Salomaa, V. (2002). *Am. J. Pathol.* **161**, 2255–2262.

Salmi, M., Tohka, S. & Jalkanen, S. (2000). *Circ. Res.* **86**, 1245–1251.

Salmi, M., Yegutkin, G. G., Lehvonen, R., Koskinen, K., Salminen, T. & Jalkanen, S. (2001). *Immunity*, **14**, 265–276.

Schwager, S. L. U., Chubb, A. J., Woodman, Z. L., Yan, L., Mentele, R., Ehlers, M. R. W. & Sturrock, E. D. (2001). *Biochemistry*, **40**, 15624–15630.

Sibon, I., Larrieu, D., El Hadri, K., Mercier, N., Feve, B., Lacolley, P., Labat, C., Daret, D., Bonnet, J. & Lamaziere, J. M. (2004). *J. Histochem. Cytochem.* **52**, 1459–1466.
Smith, D. J., Salmi, M., Bono, P., Hellman, J., Leu, T. & Jalkanen, S. (1998). *J. Exp. Med.* **188**, 17–27.
Stolen, C. M., Marttila-Ichihara, F., Koskinen, K., Yegutkin, G. G., Turja, R., Bono, P., Skurnik, M., Hänninen, A., Jalkanen, S. & Salmi, M. (2005). *Immunity*, **22**, 105–115.
Stolen, C. M., Yegutkin, G. G., Kurkijärvi, R., Bono, P., Alitalo, K. & Jalkanen, S. (2004). *Circ. Res.* **95**, 50–57.
Taylor, H. O. & Leslie, A. G. W. (1998). *Jnt CCP4/ESF–EACBM Newsl. Protein Crystallogr.* **35**, 9.
Tieleman, D. P. & Berendsen, H. J. C. (1998). *Biophys. J.* **74**, 2786–2801.
Vainio, P. J., Kortekangas-Savolainen, O., Mikkola, J. H., Jaakkola, K., Kalimo, K., Jalkanen, S. & Veromaa, T. (2005). *Basic Clin. Pharmacol. Toxicol.* **96**, 429–435.
Vidrio, H., Medina, M., Gonzalez-Romo, P., Lorenzana-Jimenez, M., Diaz-Arista, P. & Baeza, A. (2003). *J. Pharmacol. Exp. Ther.* **307**, 497–504.
Vriend, G. (1990). *J. Mol. Graph.* **8**, 52–56.
Vriend, G. & Sander, C. (1993). *J. Appl. Cryst.* **26**, 47–60.
Wilce, M. C., Dooley, D. M., Freeman, H. C., Guss, J. M., Matsunami, H., McIntire, W. S., Ruggiero, C. E., Tanizawa, K. & Yamaguchi, H. (1997). *Biochemistry*, **36**, 16116–16133.
Wilmot, C. M., Hajdu, J., McPherson, M. J., Knowles, P. F. & Phillips, S. E. V. (1999). *Science*, **286**, 1724–1728.
Wilmot, C. M., Murray, J. M., Alton, G., Parsons, M. R., Convery, M. A., Blakeley, V., Corner, A. S., Palcic, M. M., Knowles, P. F., McPherson, M. J. & Phillips, S. E. V. (1997). *Biochemistry*, **36**, 1608–1620.
Wilmot, C. M. & Thornton, J. M. (1988). *J. Mol. Biol.* **203**, 221–232.
Xiong, J.-P., Stehle, T., Zhang, R., Joachimiak, A., Frech, M., Goodman, S. L. & Arnaout, M. A. (2002). *Science*, **296**, 151–155.
Yegutkin, G. G., Salminen, T., Koskinen, K., Kurtis, C., McPherson, M. J., Jalkanen, S. & Salmi, M. (2004). *Eur. J. Immunol.* **34**, 2276–2285.
Yu, P. H., Wright, S., Fan, E. H., Lun, Z.-R. & Gubisne-Haberle, D. (2003). *Biochim. Biophys. Acta*, **1647**, 193–199.
Zorzano, A., Abella, A., Marti, L., Carpéné, C., Palacín, M. & Testar, X. (2003). *Biochem. Biophys. Acta*, **1647**, 3–9.